Croconaine Dyes with Intermediate Diradical Character Exhibiting Intense One- and Two-Photon Absorption in the Short-Wavelength Infrared Region

Taishi Oka,[a] Takeshi Maeda,*[a] Daisuke Sakamaki,[b] Hideki Fujiwara,*[b] Naoya Suzuki,[a] Shintaro Kodama,[a] Shigeyuki Yagi,[a] Luca Mauri[c,d] and Kenji Kamada[c]*

[a] Department of Applied Chemistry, Graduate School of Engineering, Osaka Metropolitan University, Naka-ku, Sakai, Osaka 599-8531, Japan

[b] Department of Chemistry, Graduate School of Science, Osaka Metropolitan University, Sumiyoshi-ku,, Osaka 558-8585, Japan

[c] Nanomaterials Research Institute (NMRI), National Institute of Advanced Industrial Science and Technology (AIST) Ikeda, Osaka 563-8577, Japan

[d] Chemistry Department**,** Università degli Studi di Milano**,** UdR dell'INSTM, Via Golgi 19, Milano 20133, Italy.

1. Experimental section

1-1. Materials and instruments

^{1}H-NMR spectra were obtained using JEOL ECX-400 spectrometers operating at 400 MHz. TG spectra were observed from RIGAKU Thermo plus EVO. Variable-temperature ESR spectra were recorded with a JEOL JES-TE-200 X-band spectrometer with a JEOL DVT2 variable-temperature unit. The electrospray ionization mass spectra (ESI-MS) were recorded on a JEOL JMS-T100CS spectrometer using CH_3OH-CH_2Cl_2 (1/1, v/v) as eluents. The absorption spectra were measured in a 1.0 or 0.10 cm quartz cell on a Shimadzu UV-3600 spectrophotometer. The elemental analyses were performed on a Yanako CHN CORDER JM-10 analyzer.

All solvents and reagents were purchased from commercial sources and used as received without further purification. Spectroscopic-grade solvents were purchased from Wako Pure Chemicals (Osaka, Japan) and used immediately after opening for all spectroscopic measurements. Crononic acid was purchased from Tokyo Chemical Industry (Tokyo, Japan). 2,6-di-phenyl-4-methylpyrylium perchlorate, 2,6-di-phenyl-4-methylthiopyrylium perchlorate and 2,6-di-phenyl-4-methylselenopyrylium perchlorate acid were prepared according to the literature.[1,2]

1-2. Synthesis and characterization

Preparation of CR2a

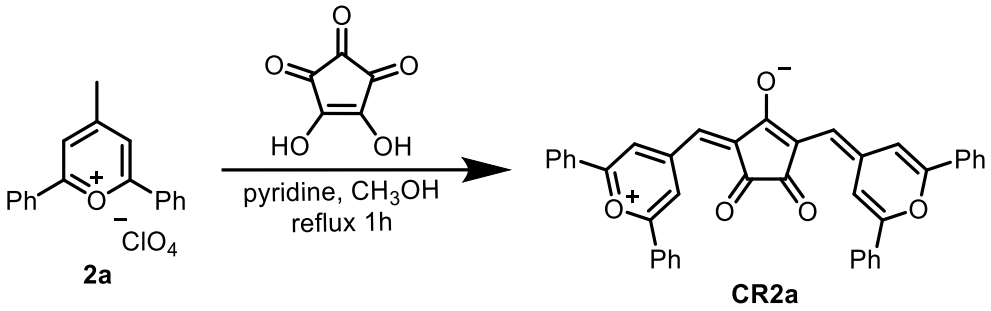

2,6-di-phenyl-4-methylpyrylium perchlorate (**2a**) (0.17 g, 0.5 mmol) and croconic acid (0.036 g, 0.25mmol) were dissolved in a mixture of CH_3OH (50 mL). Pyridine was added, and then the solution was heated under reflux for 1 hour. After cooling, the solvent was removed on a rotary evaporator, and the residue was purified by silica gel column chromatography (eluent: $CHCl_3$) to give **CR2a** (0.133 g, 0.44 mmol) as a black solid in 89% yield. ^{1}H NMR ($CDCl_3$, 400 MHz, 213K): δ 10.13-10.02 (m, 2H) 8.27-9.02 (m, 4H) 8.02–7.76 (m, 4H) 7.76-7.45 (m, 12H) 7.36-7.30 (m, 2H) 6.82-6.63 (m, 2H). HR-MS analysis: m/z = 599.1894 $[M+H]^+$, calculated from $C_{41}H_{26}O_5$, 559.1858.

Preparation of **CR2b**

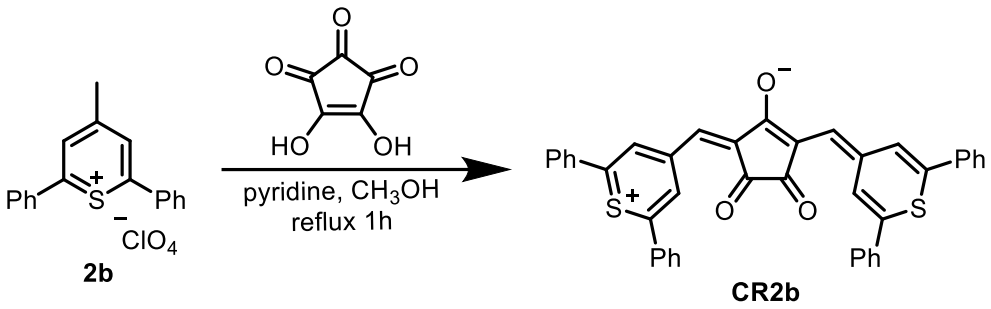

2,6-di-phenyl-4-methylthiopyrylium perchlorate (**2b**) (0.15 g, 0.4 mmol) and croconic acid (0.031 g, 0.20mmol) were dissolved in a mixture of CH_3OH (50 mL). Pyridine was added, and then the solution was heated under reflux for 1 hour. After cooling, the solvent was removed on a rotary evaporator, and the residue was purified by silica gel column chromatography (eluent: $CHCl_3$) to give **CR2b** (0.064 g, 0.101 mmol) as a black solid in 29% yield. ^{1}H NMR ($CDCl_3$, 400 MHz, 213K): δ 10.28-10.20 (m, 2H) 8.14-7.99 (m, 4H)

7.76–7.69 (m, 4H) 7.64-7.53 (m, 12H) 7.40-7.30 (m, 2H) 7.06-6.97 (m, 2H). HR-MS analysis: m/z = 630.1309 [M], calculated from $C_{41}H_{26}O_3S_2$, 630.1323.

Preparation of CR2c

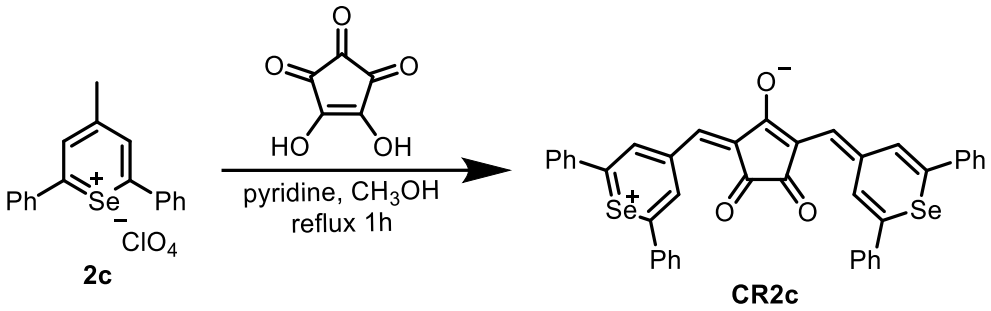

2,6-di-phenyl-4-methylselenopyrylium perchlorate (**2c**) (0.717 g, 1,75 mmol) and croconic acid (0.124 g, 0.88mmol) were dissolved in a mixture of CH_3OH (80 mL). Pyridine was added, and then the solution was heated under reflux for 1 hour. After cooling, the solvent was removed on a rotary evaporator, and the residue was purified by silica gel column chromatography (eluent: $CHCl_3$) to give **CR2c** (0.153 g, 0.211 mmol) as a black solid in 24% yield. ^{1}H NMR ($CDCl_3$, 400 MHz, 213K): δ 10.34-10.10 (m, 2H) 8.05-7.93 (m, 4H) 7.74 (m, 2H) 7.71-7.63 (m, 4H) 7.62-7.40 (m, 12H) 7.21-7.06 (m, 2H). HR-MS analysis: m/z = 724.0232 [M], calculated from $C_{41}H_{26}O_3Se_2$, 724.0233.

2. Evaluation of stability

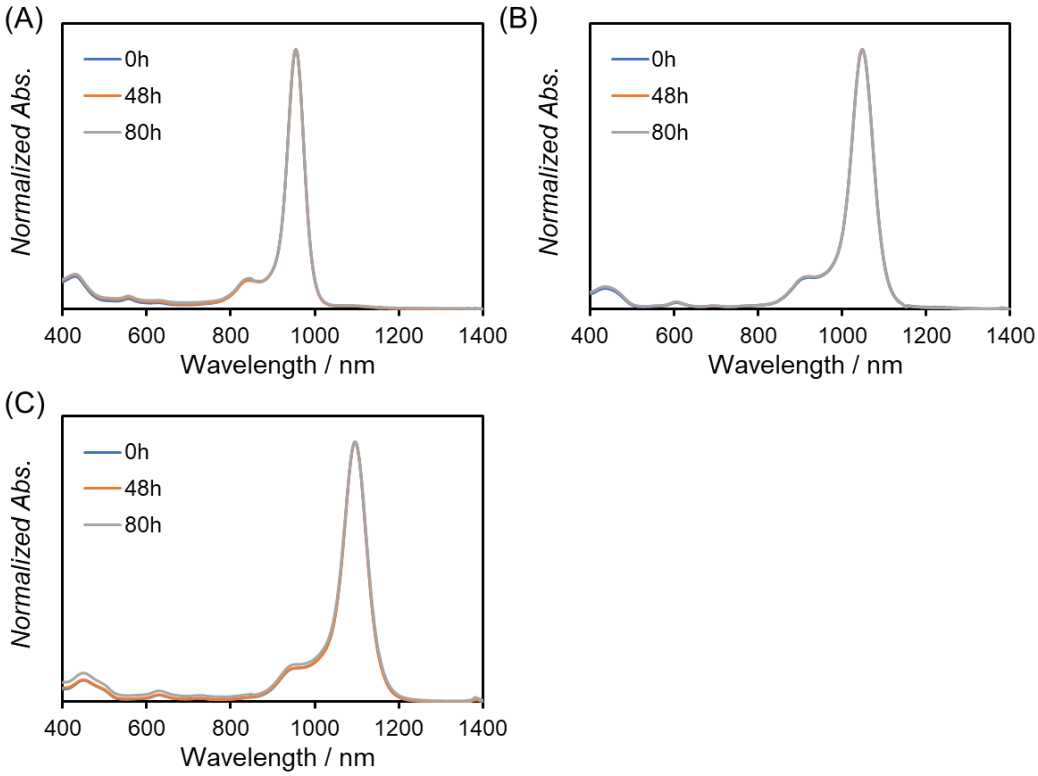

Fig. S1 Electronic absorption spectra of **CR2a** (A), **CR2b** (B), and **CR2c** (C) (100 μM in $CHCl_3$, 1-mm cuvette) measured under dark and ambient air conditions over the specified time periods.

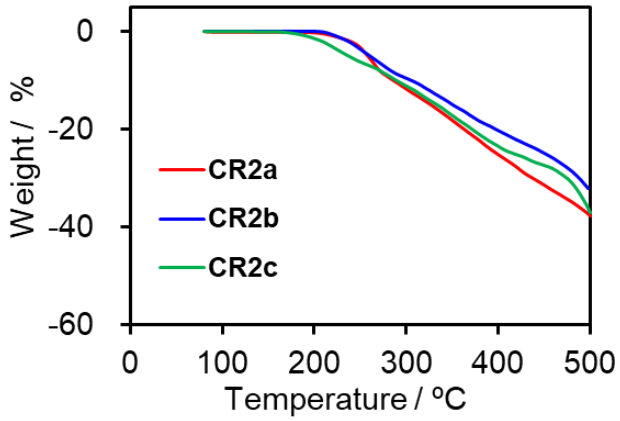

Comp.	1% weight loss temperature/ °C
CR2a	225
CR2b	224
CR2c	191

Fig. S2 Thermogravimeter-differential thermal analysis curve of **CR2a-c** at heating rate of 10 K min^{-1} under a N_2 atmosphere.

3. X-ray crystallographic analysis

Single crystals of **CR2c** were obtained by the slow diffusion of hexane into its 1,1,2,2-tetrachloroethane solution. A black block crystal of **CR2c** having approximate dimensions of 0.300 x 0.300 x 0.100 mm was used for the measurements. This crystal was mounted in a loop. All measurements were made on a Rigaku XtaLAB Synergy diffractometer using multi-layer mirror monochromated Cu-Kα radiation (λ = 1.54187 Å) at 100 K. The structure was solved by a direct methods using the SIR2004 program.[3] All the calculations were performed using the CrystalStructure 4.3 software package of the Molecular Structure Corporation.[4] 1,1,2,2-tetrachloroethane molecules contained in the crystal structure are disordered.

A summary of the crystallographic data and structure refinement is given in Table S1. Full crystallographic details excluding structure factors have been deposited at the Cambridge Crystallographic Data Centre (CCDC). CCDC-2407572 for **CR2c** contains the supplementary crystallographic data for this paper. This data can be obtained free of charge from The Cambridge Crystallographic Data Centre via www.ccdc.cam.ac.uk/data_request/cif.

Table S1. Crystallographic data for **CR2c** at 100 K.

	CR2c
Empirical Formula	$C_{45}H_{26}Cl_8O_3Se_2$
Formula Weight	1056.24
T / K	100
Color, habit	black, block
Size, mm	300 × 0.300 × 0.100
Crystal system	Triclinic
Lattice Type	Primitive
Space group	P-1 (#2)
a / Å	10.45136(18)
b / Å	13.9753(2)
c / Å	16.3849(3)
α / °	109.7451(15)
β / °	107.6675(16)
γ / °	93.0604(13)
V/ Å^3	2113.56(7)
Z	2
*D*calc / g cm^{-3}	1.660
F_{000}	1048
μ / cm^{-1}	CuKα, 71.800
2*θ*max / °	159.2
Total reflections	26817
Unique reflections	8695
Reflection/Parameter Ratio	12.21
R (*I* > 3.00σ(*I*)[a]	0.0517
*R*w (*I* > 3.00σ(*I*)[b]	0.0654
Goodness of Fit Indicator	1.089

[a]R = Σ ||*F*o| - |*F*c|| / Σ |*F*o|, [b]*R*w = [Σ w (|*F*o| - |*F*c|)^2 / Σ w *F*o^2]$^{1/2}$

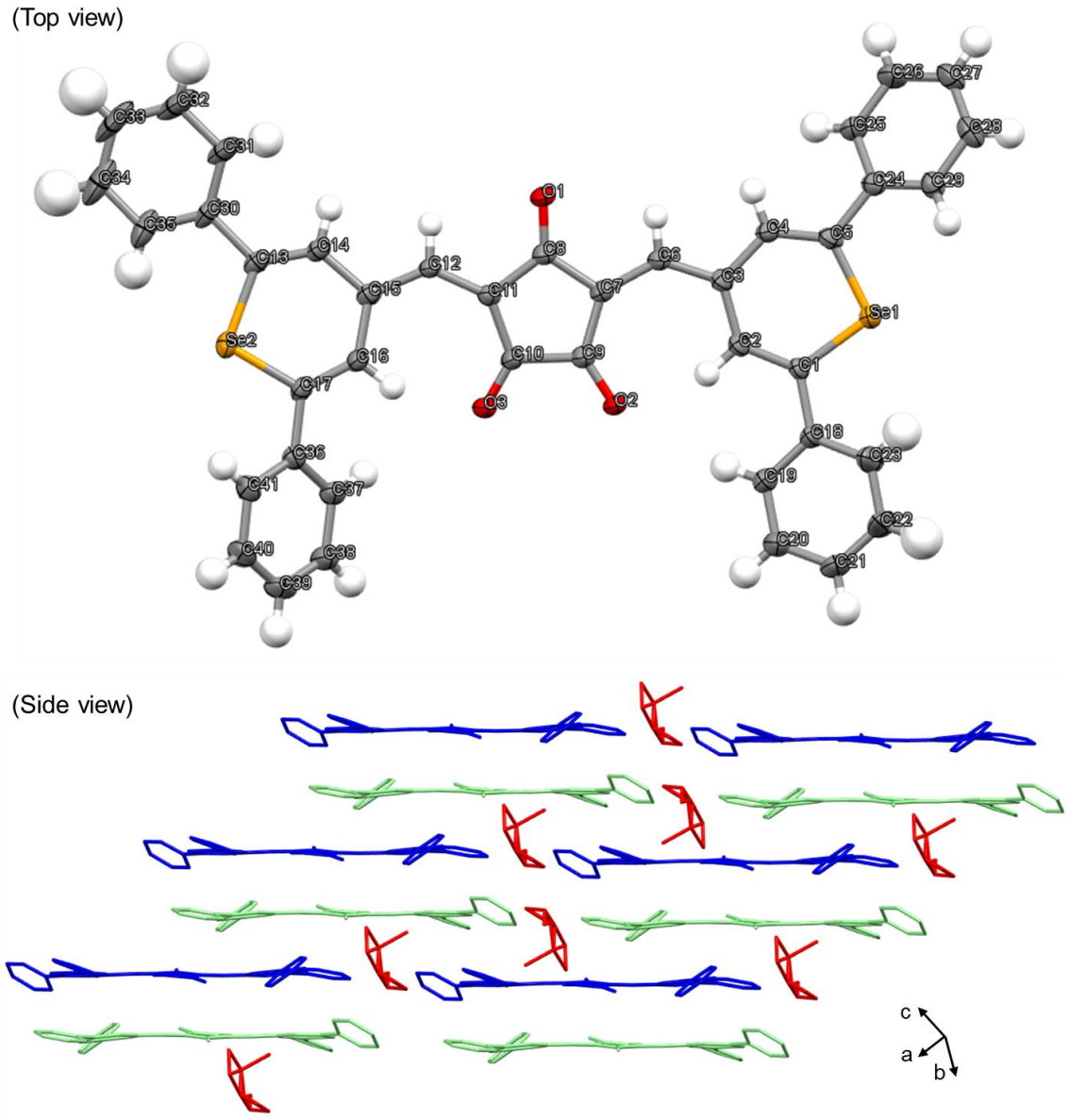

Fig. S3. A Oak Ridge thermal ellipsoid program drawing (A) and a crystal packing (B) of **CR2c**.

Table S2. Representative C-C and C-Se bond lengths of the single crystal of **CR2c** at 100 K.

bond	length (Å)	bond	length (Å)
Se1-C1	1.883	Se2-C13	1.89
Se1-C5	1.878	Se2-C17	1.877
C1-C2	1.367	C13-C14	1.350
C2-C3	1.425	C14-C15	1.440
C3-C4	1.428	C15-C16	1.435
C4-C5	1.354	C16-C17	1.350
C3-C6	1.414	C15-C12	1.409
C6-C7	1.393	C12-C11	1.399
C7-C8	1.475	C11-C8	1.477
C8-O1	1.234		

4. Resonance structures

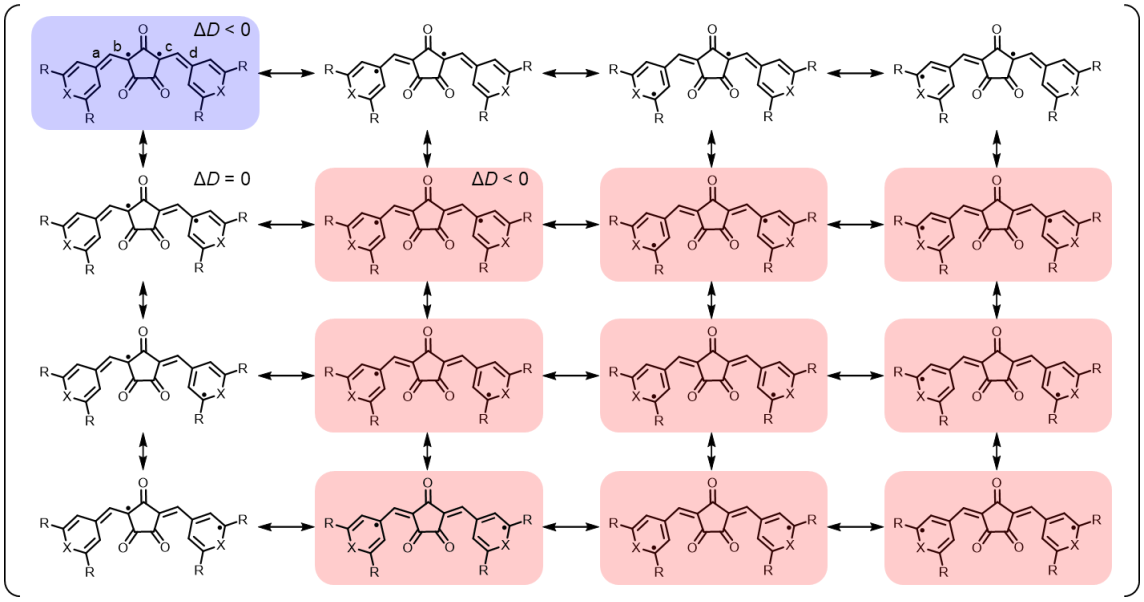

Fig. S4. A resonance structure for the diradical form of present croconaine dyes. Glay and red backgrounds indicate resonance forms with $\Delta D < 0$ and $\Delta D > 0$, respectively. ΔD is defined in the main text as following equation: ΔD = ave. (*a*, *d*) – ave. (*b*, *c*).

5. Variable temperature ^{1}H NMR spectra

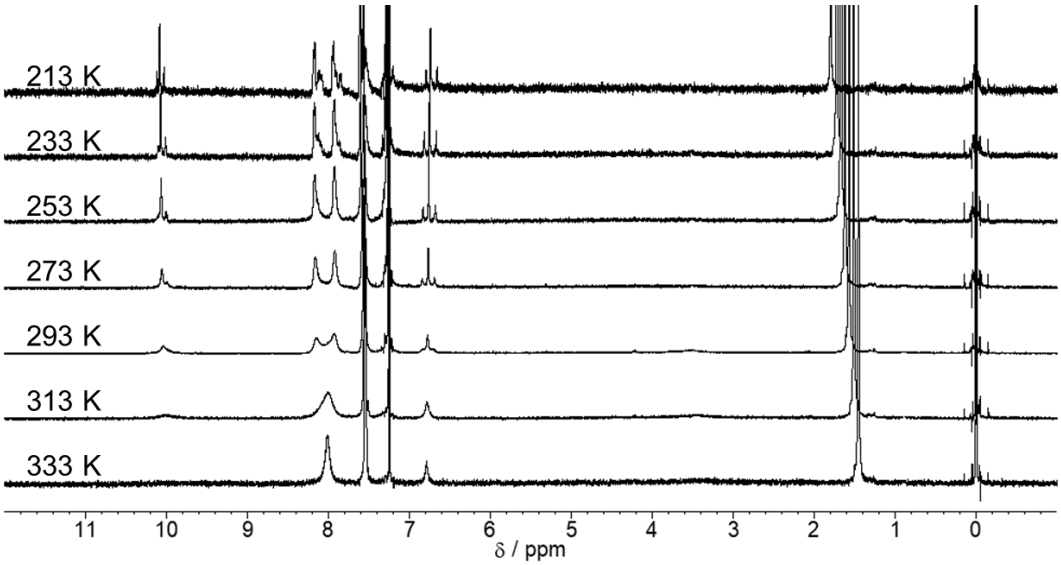

Fig. S5 Variable temperature ^{1}H NMR spectra ($CDCl_3$, 213 K-333 K) of **CR2a.**

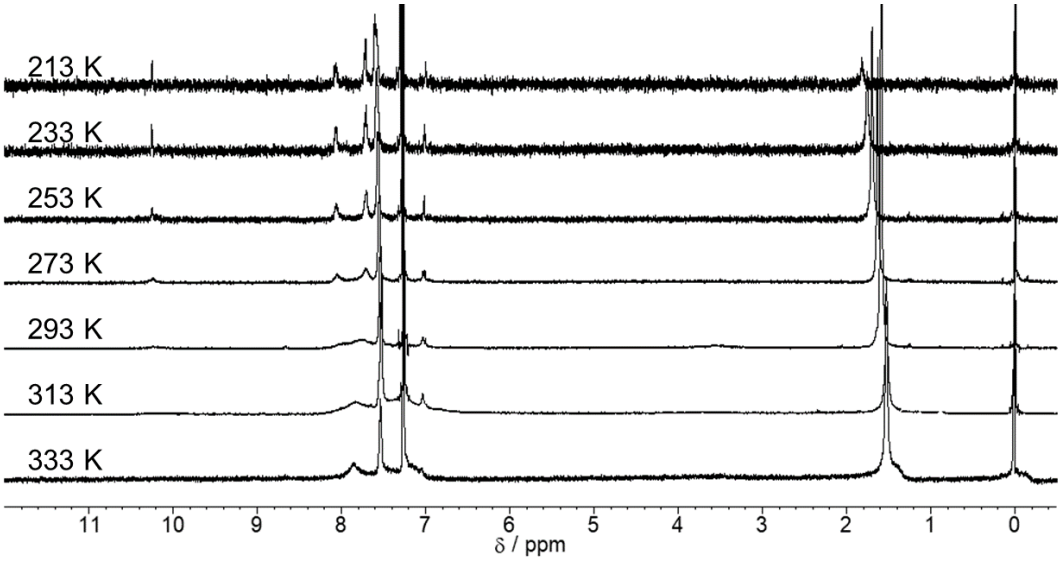

Fig. S6 Variable temperature ^{1}H NMR spectra ($CDCl_3$, 213 K-333 K) of **CR2b**.

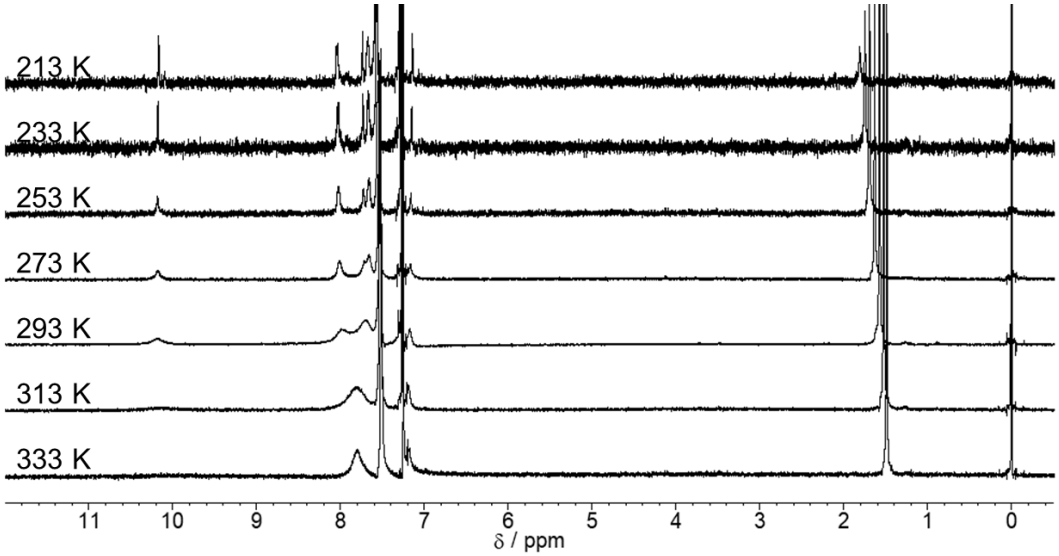

Fig. S7 Variable temperature ^{1}H NMR spectra of **CR2c** in $CDCl_3$ (213 K-333 K).

6. Variable temperature ESR spectra

The variable temperature (VT) ESR spectra were measured on a JEOL JES-TE-200 X-band spectrometer with a JEOL DVT2 variable-temperature unit. The temperature dependency of ESR intensities (I_{ESR}) of present dyes in the solid state was fitted by modified Bleaney–Bowers equation[5]:

$$I_{ESR}\,T = \frac{C}{3+exp(-\Delta E_{S-T}/k_B T)}$$

Where I_{ESR} is the ESR intensity, T is the temperature, C is a constant, k_B is Boltzman's constant, and $\Delta E_{S\text{-}T}$ is an energy gap between the singlet ground state to the triplet excited state.

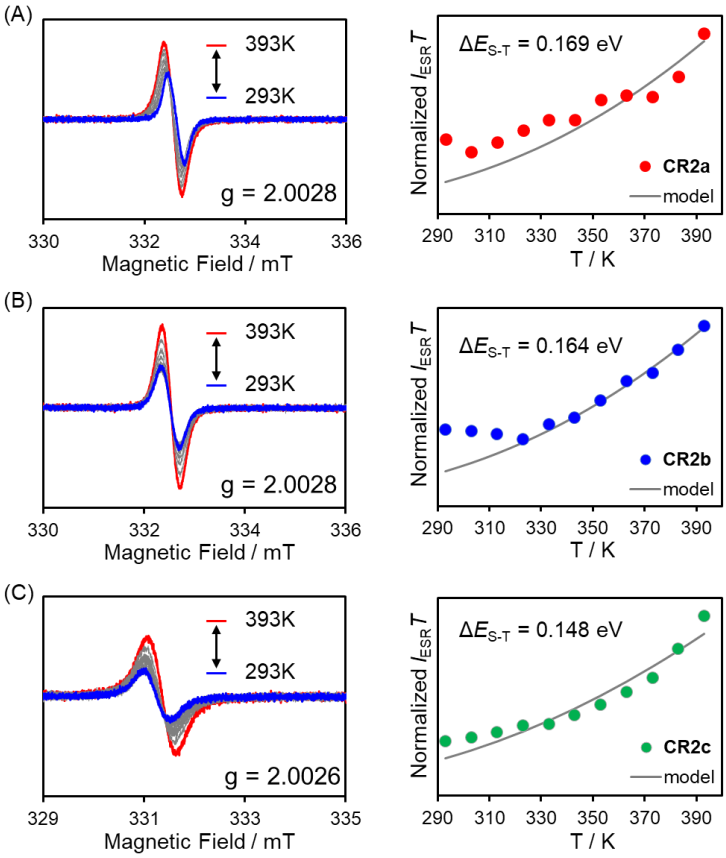

Fig. S8 ESR spectra of **CR2a** (A, g = 2.005), **CR2b** (B, g = 2.005), **CR2c** (C, g = 2.001) in 1,1,2,2-tetrachloroethane and temperature- $I_{ESR}T$ plots based on ESR data of **CR2a** (red), **CR2b** (blue), and **CR2c** (green); the dotted lines are the fitted plots by using Bleaney–Bowers equation.

7. Two-photo absortion measurement

Two-photon absorption (TPA) spectra of the sample solutions were measured by the open-aperture Z-scan methods,[6] in which nonlinear absorption (NLA) was detected as decrease of transmittance of the focused laser beam through sample near and at the focal point by scanning the sample along the beam. A femtosecond optical parametric amplifier (*Spectra-Physics Topas Prime*, pumped by a Ti:S regenerative amplifier operating at repetition rate f = 1 kHz) was used as light source by changing the optical configuration depending on the wavelength. The details of setup were described elsewhere.[7] The measurement gives open-aperture Z-scan trace, i.e., a transmittance curve as a function of sample position with a dip at focal point when NLA exists. The transmittance is normalized to that at the sample position far enough from the focal point. The obtained open-aperture Z-scan traces were analyzed with the theoretical formular assuming the spatial and temporal Gaussian pulsed beam attenuated only by TPA process.[7]

$$T_N(\zeta) = \frac{1}{\sqrt{\pi}\ q(\zeta)} \int_{-\infty}^{\infty} \ln\left[1 + q(\zeta) e^{-x^2}\right] dx,$$

where two-photon absorbance $q(\zeta) = q_0/(1+\zeta^2)$ and the normalized transmittance T_N ($T_N = 1$ for $|\zeta| \gg 1$) are function of the normalized sample position $\zeta = z/z_R$. The Rayleigh range z_R was 5–8 mm depending on the wavelength, which was much longer than optical pathlength L of the sample and the thin sample condition necessary for the analysis was hold. On-axis two-photon absorbance at the focal point q_0 was obtained from the curve fit. TPA coefficient of the sample $\alpha^{(2)}$was obtained from the convention $q_0 = \alpha^{(2)} I_0 L_{\text{eff}}$, where $I_0 = 4(\ln 2)^{1/2} P/(\pi^{3/2} w_0^2 t_p f)$ is the peak on-axis intensity of incident laser pulse at the focal point ($z = 0$), P is average input power, $w_0 = (z_R \lambda/\pi)^{1/2}$ is beam waist radius, λ is the incident wavelength, t_p is the laser pulse width in FWHM obtained by the autocorrelator (APE, *PulseCheck*). Good fitting to autocorrelation was obtained by Gaussian pulse model for each λ. t_p =76–96 fs depending on λ. L_{eff} is the effective pathlength of the sample defined as $L_{\text{eff}} = (1 - 10^{-A})L/(A \ln 10)$ with A is absorbance (one-photon absorption) of the sample at the incident wavelength. TPA coefficient $\sigma^{(2)}$ was calculated with $\sigma^{(2)} = h\nu N^{-1} \alpha^{(2)}$, where N is number density calculated from sample concentration and $h\nu$ is the photon

energy. $\sigma^{(2)}$ was expressed in the Göppert-Mayer (GM) unit defined as 1 GM = 10^{-50} cm^4 s $molecule^{-1}$ $photon^{-1}$.

TPA spectral measurement by the Z-scan method were performed in two different procedures; one is that measurement was repeated by changing wavelength at a fixed incident power (referred as *wavelength scan*). The other is that measurement was repeated for different incident power for each wavelength (referred as *power scan*). We employed *wavelength scan* to obtain outline of the spectral shape and then did power scan to confirmed that the obtained NLA signal was originated from TPA process by checking proportionality of q_0 and I_0). Typical open-aperture Z-scan traces and the proportionality plots of the samples are shown in Figs. S9–11. The concentrations were 0.44 mM for **CR2a**, 0.49 mM for **CR2b**, and 0.47 mM for **CR2c**. The solvent was spectroscopic grade $CHCl_3$ for all. The obtained values of $\sigma^{(2)}$ were corrected by using the standard compounds measured at the same time (PAB101 (Compound **4** in ref. 7) in CH_2Cl_2 for 1200–1600 nm).

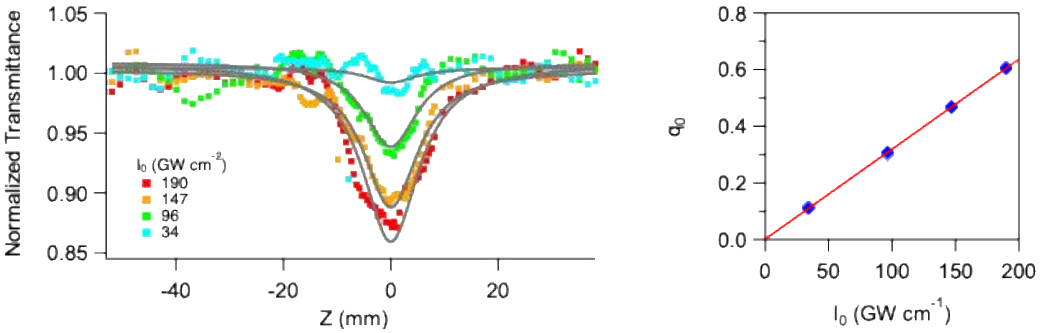

Fig. S9. (left) Open-aperture Z-scan traces of **CR2a** in $CHCl_3$ (0.44 mM) at 1255 nm with different on-axis peak intensities I_0 (squares) with theoretical fits (grey curves). (right) Plot of two-photon absorbance q_0 obtained by the curve fitting against I_0.

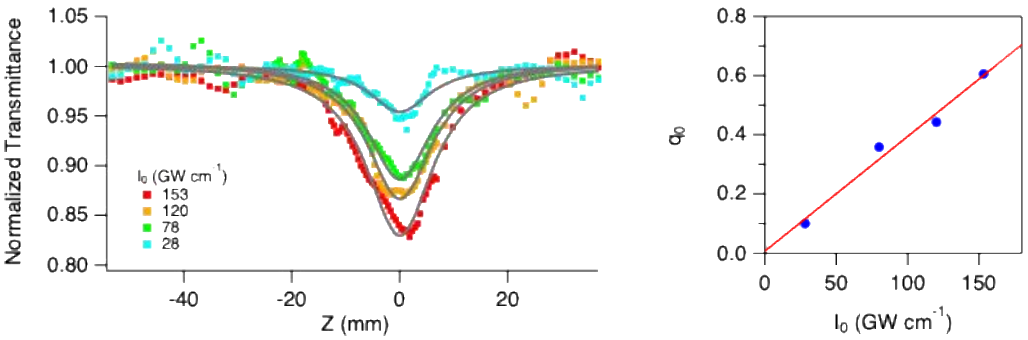

Fig. S10. (left) Open-aperture Z-scan traces of **CR2b** in $CHCl_3$ (0.49 mM) at 1395 nm with different on-axis peak intensities I_0 (squares) with theoretical fits (grey curves). (right) Plot of two-photon absorbance q_0 obtained by the curve fitting against I_0.

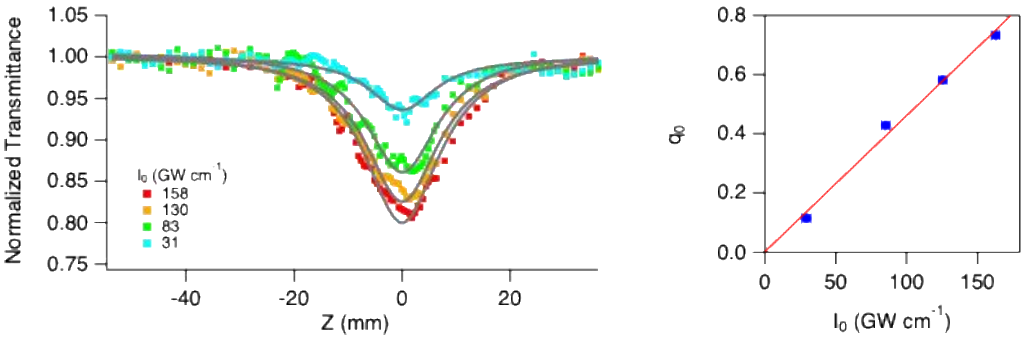

Fig. S11. (left) Open-aperture Z-scan traces of **CR2c** in $CHCl_3$ (0.47 mM) at 1454 nm with different on-axis peak intensities I_0 (squares) with theoretical fits (grey curves). (right) Plot of two-photon absorbance q_0 obtained by the curve fitting against I_0.

8. Spectral simulation by quantum chemical calculation

Quantum chemical calculations of the compounds were performed for spectral simulation of one- and two-photon absorptions（OPA and TPA, respectively）by using Gaussian16 programming package.[8] Geometry optimization, time-dependent, and the Tamm–Dancoff approximation (TDA)[9] calculations were performed at the CAM-B3LYP/6-31G(d,p) level of theory. Coordinates of the optimized geometries are shown in Section 11. TDA calculations gave the transition energies ($E_{kg} = \hbar\omega_{kg}$ or $E_{fg} = \hbar\omega_{fg}$ here $\hbar$ is the reduced Planck constant) from the ground state g to the excited states, which can act as an intermediate state k or the destination (final) state f, transition dipole moments from g to k or f (μ_{kg}, μ_{fg}), those from k to f (μ_{fk}), and differences in permanent dipole moments between g and f ($\Delta\mu_{fg}$), which are needed for the spectral simulation. The calculation method of TPA cross section $\sigma^{(2)}$ using them has been reported previously,[10] and is briefly described here. The $\sigma^{(2)}$ at angular frequency ω of incident photon ($\omega = 2\pi c/\lambda$ for the incident wavelength λ with the speed of light c) is expressed as,

$$\sigma^{(2)}(\omega) = \frac{4\pi^3\omega^2}{c^2n^2}\langle|\mathbf{M}_{fg}^{(2)}|^2\rangle\ g(2\omega)\ ,$$

where

$$g(2\omega) = \frac{1}{\pi}\ \frac{\Gamma_{fg}}{\left(\omega_{fg} - 2\omega\right)^2 + \Gamma_{fg}^2}$$

is the normalized Lorentzian line-shape function with a dumping constant (i.e., linewidth of the TPA peak) Γ_{fg}. n is the refractive index. $\mathbf{M}_{fg}^{(2)}$ is the two-photon transition matrix element between g and f. The orientationally averaged TPA probability $\langle|\mathbf{M}_{fg}^{(2)}|^2\rangle$ can be divided into the following three terms as,

$$\langle|\mathbf{M}_{fg}^{(2)}|^2\rangle = T_{\text{three-state}} + T_{\text{dipolar}} + T_{\text{cross}}\ ,$$

where

$$T_{\text{three-state}} = \frac{4}{15\hbar^2}\left[\sum_{k\neq g,f}\sum_{k'\neq g,f}\frac{1}{(\omega_{kg}-\omega)(\omega_{k'g}-\omega)}\right.$$
$$\times\{\ (\mu_{fk}\cdot\mu_{kg})(\mu_{fk'}\cdot\mu_{k'g})+(\mu_{fk}\cdot\mu_{k'g})(\mu_{fk'}\cdot\mu_{kg})$$
$$\left.+(\mu_{fk}\cdot\mu_{fk'})(\mu_{kg}\cdot\mu_{k'g})\}\right],$$

$$T_{\text{dipolar}} = \frac{4}{15\hbar^2}\frac{|\Delta\mu_{fg}|^2|\mu_{fg}|^2}{\omega^2}(1+2\cos^2\phi)$$

where ϕ is the angle between $\Delta\mu_{fg}$ and μ_{fg}, and

$$T_{\text{cross}} = \frac{8}{15\hbar^2}\left[\sum_{k\neq g,f}\frac{1}{\omega(\omega_{kg}-\omega)}\{\ (\mu_{fk}\cdot\mu_{kg})(\Delta\mu_{fg}\cdot\mu_{fg})\right.$$
$$\left.+(\mu_{fk}\cdot\mu_{fg})(\Delta\mu_{fg}\cdot\mu_{kg})+(\mu_{fg}\cdot\mu_{kg})(\Delta\mu_{fg}\cdot\mu_{fk})\}\right].$$

Here, "·" is the dot product operators between two dipole moments, which are three-dimensional vector. $T_{\text{three-state}}$ is the three-state term and corresponds to the three-state model where two intermediate states are not neither the ground nor final states of the TPA transition ($k,k'\neq g,f$) while T_{dipolar} is the dipolar term and corresponds to the two-state model where k is g or f. For centrosymmetric molecules, $\Delta\mu_{fg}=0$ and therefore $T_{\text{dipolar}}=0$. T_{cross} is the cross term between the three-state and dipolar terms and $T_{\text{cross}}=0$ also for centrosymmetric molecules.

For the spectral simulation, we considered the ground state (S_0) and 20 excited states (S_1–S_{20}) for k and f. Solvent effect was considered by using polarizable continuum model (PCM) for $CHCl_3$. Note that these calculations do not include the contribution of double excitation. The obtained TPA spectra together with the OPA spectra are shown in Fig. S12(A)-(C). The empirical relaxation constants for one- and two-photon resonance were chosen to be 0.1 eV. The electronic configuration of the first four excited states is listed in Table S3. For all compounds, $S_0\rightarrow S_1$ transition is strongly OPA allowed (dominated by HOMO→LUMO transition) and $S_0\rightarrow S_2$, $S_0\rightarrow S_3$, and $S_0\rightarrow S_3$ transitions are very weak or negligible as shown by the oscillator strengths. For all compounds, a strong TPA peak is located at high energy side of the OPA peak. The TPA peak originates

from $S_0 \rightarrow S_4$ transition (HOMO→LUMO+1 transition). Decomposed TPA spectra by the symmetry terms (Fig. S12(D)-(F)) show that $T_{\mathrm{three-state}}$ is dominant for all. This means that the compounds can be regarded as centrosymmetric and their TPA spectra can be interpreted by the three-state model. Decomposed spectra by destination state f (Fig. S12(G)-(I)) show that $S_0 \rightarrow S_4$ is strongly allowed TPA transition and $S_0 \rightarrow S_{11}$ is weakly allowed TPA transition. Thus, S_2 (HOMO-1→LUMO) and S_3 (HOMO-4 (or HOMO-5 for **CR2c**)→LUMO) are dirk state for both OPA and TPA.

$T_{\mathrm{three-state}}$ can be simplified further as follows for the case that $k = k'$ is dominant (so-called diagonal approximation),

$$T'_{\mathrm{three-state}} = \sum_{k \neq g,f} \frac{4}{15\hbar^2} \frac{\left|\mu_{fk}\right|^2 \left|\mu_{kg}\right|^2}{\left(\omega_{kg} - \omega\right)^2} (1 + 2\cos^2\theta_k)$$

where θ_k is the angle between the two transition dipole moments μ_{fk} and μ_{kg}. The $\sigma^{(2)}$ at the peak of $g \rightarrow f$ transition ($\omega = \omega_{fg}$) is written as the sum of the components over k as

$$\sigma^{(2)}\left(\frac{\omega_{fg}}{2}\right) = \sum_{k \neq g,f} \sigma_k^{(2)}\left(\frac{\omega_{fg}}{2}\right)$$

and each component is

$$\sigma_k^{(2)}\left(\frac{\omega_{fg}}{2}\right) \propto \left|\mu_{fk}\right|^2 \left|\mu_{kg}\right|^2 \times \left(\frac{\hbar\omega_{kg}}{\hbar\omega_{fg}/2} - 1\right)^{-2} \times (1 + 2\cos^2\theta_k)$$

under the diagonal approximation (i.e., $T'_{\mathrm{three-state}}$ is dominant). Furthermore, only one k is usually considered (the single-intermediate-state approximation, i.e., $\sigma^{(2)}(\omega_{fg}) \approx \sigma_k^{(2)}(\omega_{fg})$) for interpreting the experimental data because of simplicity. From the above equation, both $\left|\mu_{fk}\right|$ and $\left|\mu_{kg}\right|$ must be large as the essential requirement to obtain a large $\sigma^{(2)}$. For the TPA peak of $S_0 \rightarrow S_4$ transition ($g = 0$ and $f = 4$), S_1 ($k = 1$) is the dominant intermediate state. Its orbital transition path is HOMO → LUMO → LUMO+1 because HOMO → LUMO corresponds to μ_{10} ($S_0 \rightarrow S_1$) and LUMO → LUMO+1 corresponds to μ_{41} ($S_1 \rightarrow S_4$). As shown in Fig. S13, HOMO and LUMO overlap throughout molecule and LUMO and LUMO+1do the same. These can give large μ_{10} and μ_{41}. For other transitions such as $S_0 \rightarrow S_2$ and $S_0 \rightarrow S_3$, their orbital paths are, respectively, HOMO−1 → HOMO → LUMO and HOMO−4 (or −5) → HOMO →

LUMO. These have poor orbital overlaps between HOMO−1 → HOMO or HOMO−4 (or -5) → HOMO because HOMO−1 and HOMO−4 (or −5) have orbital at the center of molecule while HOMO has extended orbital throughout molecule. This qualitative consideration is supported by the oscillator strengths in Table S3, which means that μ_{10} is much larger than μ_{20} and μ_{30}.

More quantitative results are summarized in Table S4 where not only the squared product of the transition dipole moment $DMP = |\mu_{fk}|^2 |\mu_{kg}|^2$ but also the angle factor $1 + 2\cos^2\theta_k$ and the detuning factor $DF = \left(\frac{\hbar\omega_{kg}}{\hbar\omega_{fg}/2} - 1\right)^{-2}$ are considered. However, the conclusions are the same as that of the qualitative discussion above. The $S_0 \rightarrow S_4$ TPA transition is strong because both $|\mu_{fk}|$ and $|\mu_{kg}|$ are large (respectively, 12–13 D and 22–24 D) while the TPA transitions to other excited states are weak or negligible because $|\mu_{fk}|$ is very small (0–3 D) for $S_2 - S_6$ (except S_4, of course). The TPA transition to S_1 is also very weak. In this case, S_{11} is the k that gives the largest cross section magnitude (RM in Table S4). Because $k = 11$ is located much higher than $f = 1$, the value of *DF* is very small compared to others although $|\mu_{fk}|$ and $|\mu_{kg}|$ are moderate values (respectively, 4–5 D and 7–10 D).

Table S3. Transition energy (*E*) and wavelength (λ), oscillator strength, and major orbital transition path and its contribution (in parentheses) of the first four excited states of each compound calculated at the TDA-PCM ($CHCl_3$)-CAM-B3LYP/6-31-G(d,p) level.

Cmpnd.	State	*E*/eV (λ/nm)	Osc. Str.	Orb. Contribution
CR2a	1	1.4350 (864.0)	2.54381	H → L (0.69089)
	2	2.5661 (483.1)	0.0001	H-1 → L (0.67568)
	3	2.8818 (430.2)	0.0004	H-4 → L (0.68310)
	4	2.9815 (415.8)	0.0140	H → L+1 (0.67380)
CR2b	1	1.2691 (976.94)	2.5590	H → L (0.69215)
	2	2.4762 (500.71)	0.0015	H-1 → L (0.67109)
	3	2.8020 (442.49)	0.0004	H-4 → L (0.67069)
	4	2.8647 (432.79)	0.0082	H → L+1 (0.67155)
CR2c	1	1.2104(1024.36)	2.5849	H → L (0.69251)
	2	2.4463(506.82)	0.0015	H-1 → L (0.66139)
	3	2.7761(446.61)	0.0006	H-5 → L (0.67410)
	4	2.8216(439.41)	0.0067	H → L+1 (0.66435)

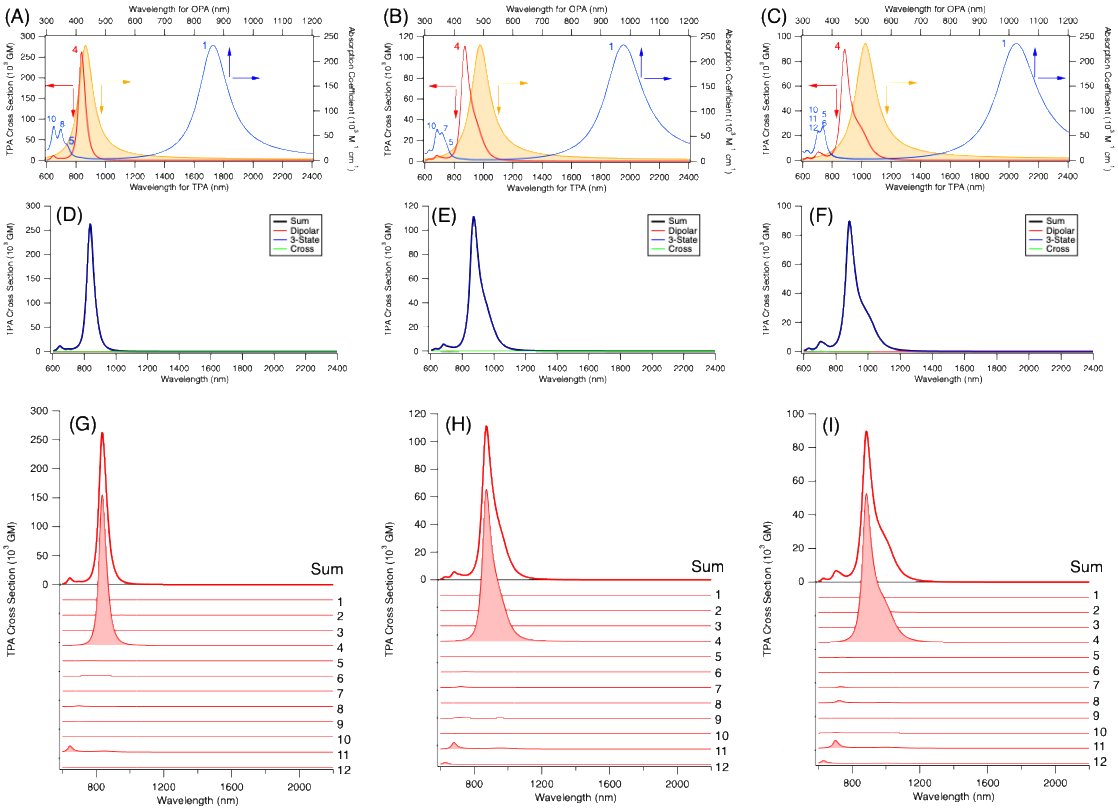

Fig. S12. Simulated TPA spectra (red: bottom and left axes) and OPA spectra (orange: bottom and right axes; blue: bottom and top axes) of (A) **CR2a**, (B) **CR2b**, and (C) **CR2c**. The top and bottom axes are scaled so that TPA and OPA peaks (in red and blue) having the same transition energies are located at the same position. The numbers next to peaks designate the destination excited states by the TPA (red) and OPA (blue) transitions. The calculations were done at the TDA-PCM ($CHCl_3$)-CAM-B3LYP/6-31-G(d,p) level up to 20th excited states. In the middle row, decomposed TPA spectra by symmetry terms for (D) **CR2a**, (E) **CR2b**, and (F) **CR2c** are shown. In the bottom row, decomposed TPA spectra by destination state (thin line) of (G) **CR2a**, (H) **CR2b**, and (I) **CR2c** are shown. The numbers in the panels (1, 2, 3…) mean destination state, i.e., TPA transition components of $S_0 \rightarrow S_1$, $S_0 \rightarrow S_2$, $S_0 \rightarrow S_3$ … , respectively.

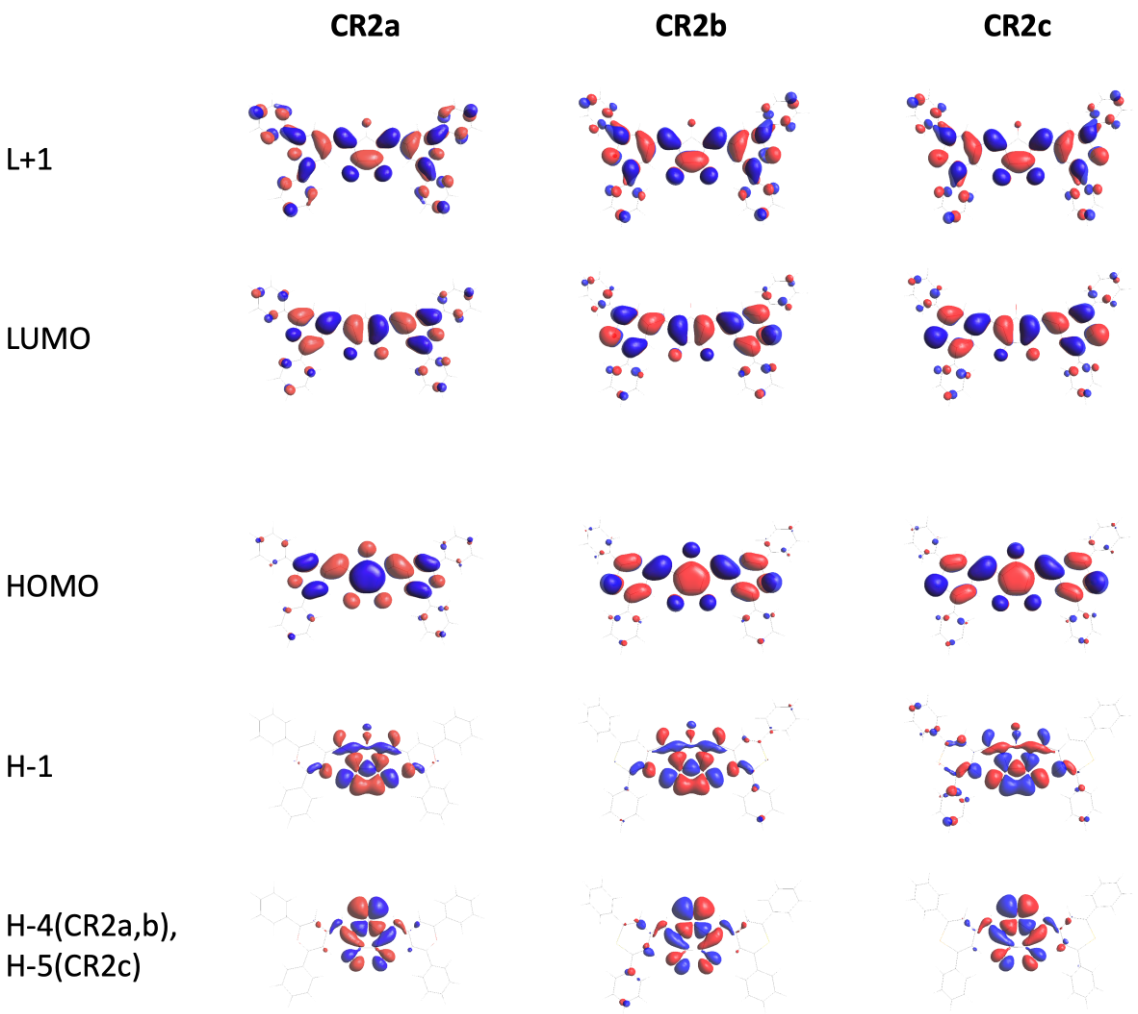

Fig. S13. Orbital patterns of the compounds calculated at the CAM-PCM($CHCl_3$)-B3LYP/6-31-G(d,p) level.

Table S4. Parameters related to the major TPA transition paths obtained by the DFT calculation (CAM-B3LYP/6-31+G(d) with PCM ($CHCl_3$)) for 20 excited states. μ_{kg} is transition dipole moment from the ground state $g = 0$ to excited state *k*. μ_{fk} is transition dipole moment from *k* to the destination state *f* (μ_{fk}), their square product ($DMP = \left|\mu_{fk}\right|^2\left|\mu_{kg}\right|^2$), the angle between them (θ_k), and detuning factor $DF = \left(\frac{E_{kg}}{E_{fg}/2} - 1\right)^{-2}$. The relative magnitude of TPA cross section is $RM = DMP \times DF \times (1 + 2\cos^2\theta_k)$. The *k* that gives the largest value of RM is chosen for each row.

Cpd.	*k*	$\left\|\mu_{kg}\right\|$ / D	*f*	$\left\|\mu_{fk}\right\|$ / D	*DMP* / 10^4 D^4	θ_k / °	*DF*	*RM* /10^5
CR2a	11	3.7	1	9.6	0.12	90.0	0.05	0.0007
	1	**21.6**	2	0.4	0.01	7.5	71	0.2
			3	0.0	0.00	86.2	59643	0.07
			4	**12.4**	**7.21**	**0.2**	**715**	**1548**
			5	0.7	0.02	1.8	48	0.3
			6	2.7	0.32	90.1	47	1.5
CR2b	11	3.7	1	7.4	0.07	74.3	0.04	0.0004
	1	**21.6**	2	0.5	0.02	–47.2	1595	5
			3	0.8	0.03	2.7	112	1
			4	**13.2**	**9.24**	**–0.3**	**77**	**213**
			5	1.0	0.05	53.8	18	0.1
			6	2.2	0.03	–85.8	17	0.5
CR2c	11	4.9	1	6.6	0.10	–8.4	0.04	0.001
	1	**23.7**	2	0.6	0.02	–44.7	9203	36
			3	1.0	0.06	1.9	61	1
			4	**13.6**	**10.47**	**–0.2**	**50**	**156**
			5	0.9	0.05	59.3	13	0.09
			6	1.3	0.10	69.2	13	0.2

9. Comparison of optical properties of squaraine and croconaine dyes

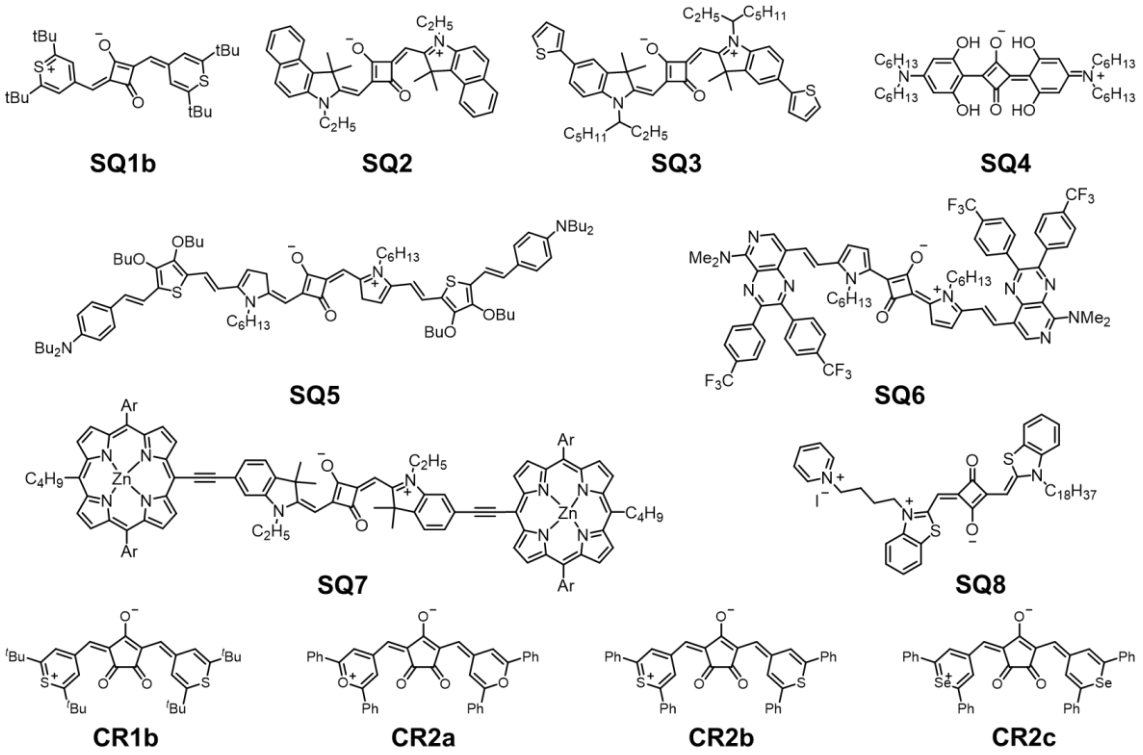

Fig. S14 Structures of single-chromophore squaraine dyes exhibiting two-photon absorption properties showed in Fig. 10 in the main text and Table S5.

Table S5. OPA and TPA properties of squaraine and croconaine dyes with a single chromophore of structurally similar oxocarbon analogues were investigated, focusing on molecules exhibiting TPA properties above 1000 nm.

Molecules	λ_{OPA} (nm)	λ_{TPA} (nm)	$\sigma^{(2)}$ (GM)	M.w.	$\sigma^{(2)}$ / M.w.	Solvent	Rate-method	Ref.
SQ1b	810	1100	370	522.81	0.708	CLF	fs-z-scan	11
SQ2	624	1250	650	552.72	1.176	EtOH	fs-z-scan	12
SQ3	646	1240	483	785.16	0.615	Toluene	ns-TPEF	13
SQ4	650	1200	1000	664.93	1.504	THF	fs-z-scan	14
SQ5	832	1500	800	1372.06	0.583	DCM	ns-TPEF	15
SQ6	764	1640	704	1353.37	0.520	CFL	fs-z-scan	16
SQ7	732	1500	2000	1512.03	1.323	THF	ns-TPEF	17
SQ8	641	1000	280	890.04	0.315	Toluene	ns-TPEF	18
CR1b	954	1310	750	550.82	1.362	CLF	fs-z-scan	11
CR2a	955	1255	1008	598.65	1.684	CLF	fs-z-scan	-
CR2b	1047	1395	1010	630.78	1.601	CLF	fs-z-scan	-
CR2c	1096	1454	1177	724.6	1.624	CLF	fs-z-scan	-

10. **NMR and MS spectra**

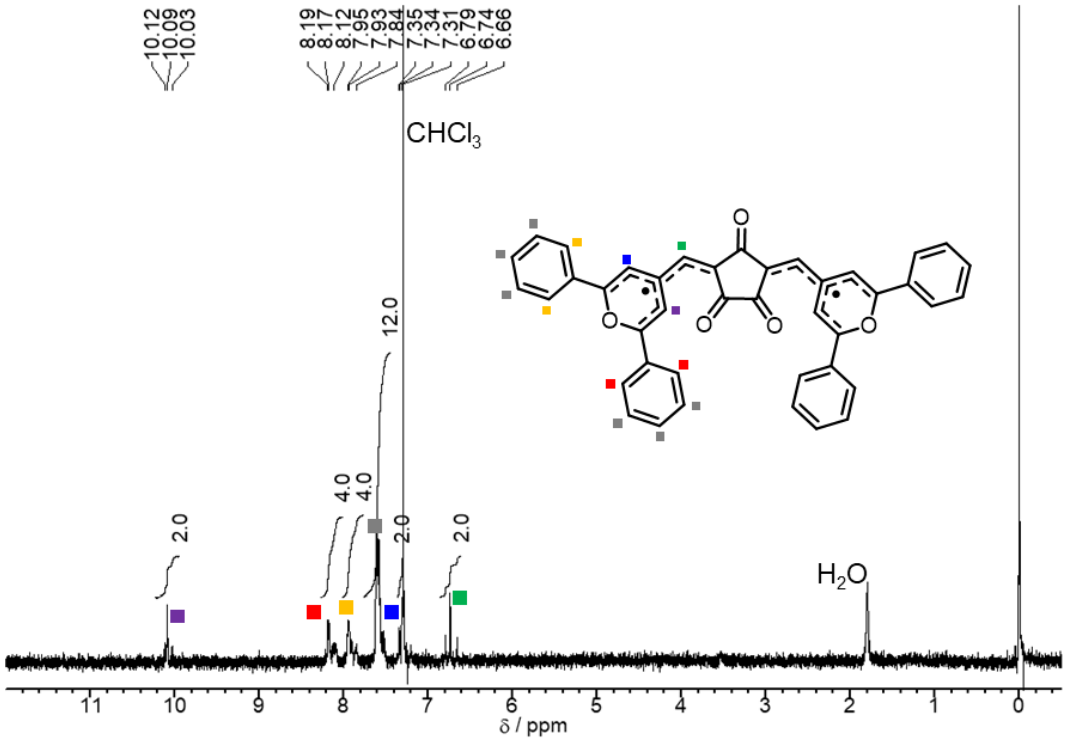

Fig. S15 ^{1}H NMR spectrum ($CDCl_3$, 213K) of **CR2a**.

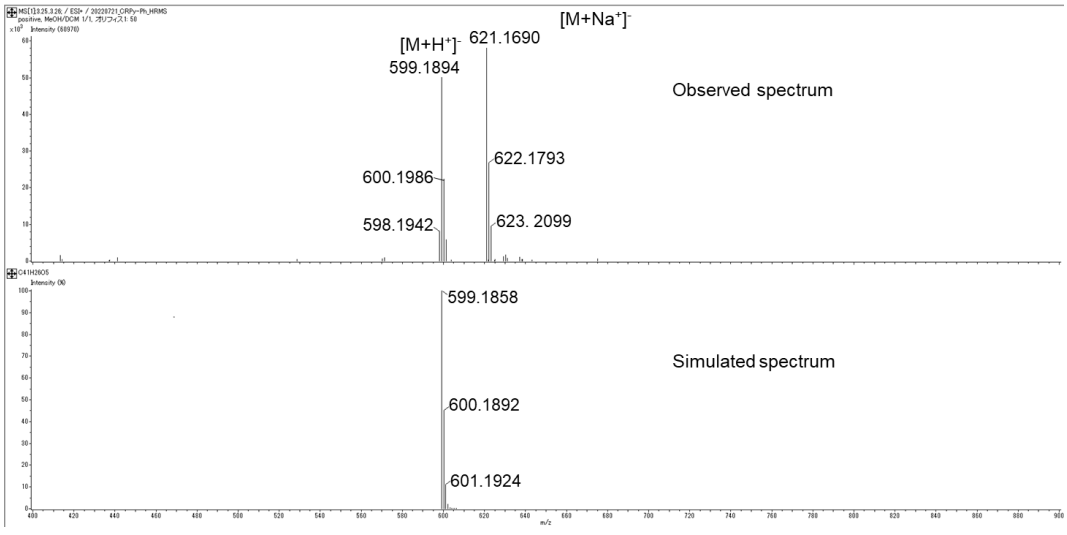

Fig. S16 ESI-MS spectrum of **CR2a** (top) and its corresponding simulated spectrum (bottom).

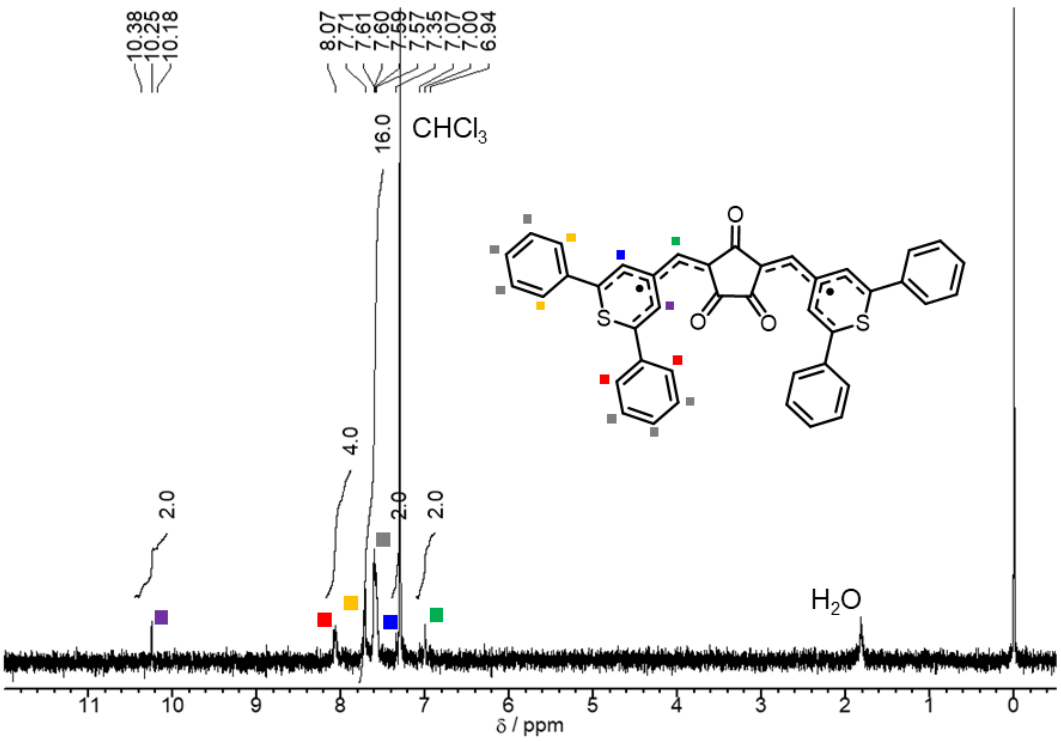

Fig. S17 ^{1}H NMR spectrum ($CDCl_3$, 213K) of **CR2b**.

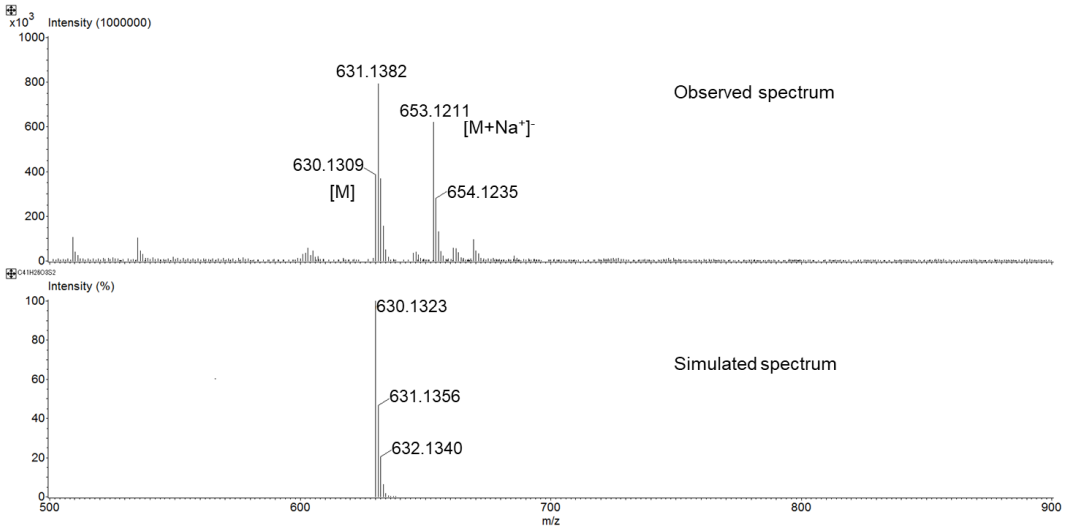

Fig. S18 ESI-MS spectrum of **CR2b** (top) and its corresponding simulated spectrum (bottom).

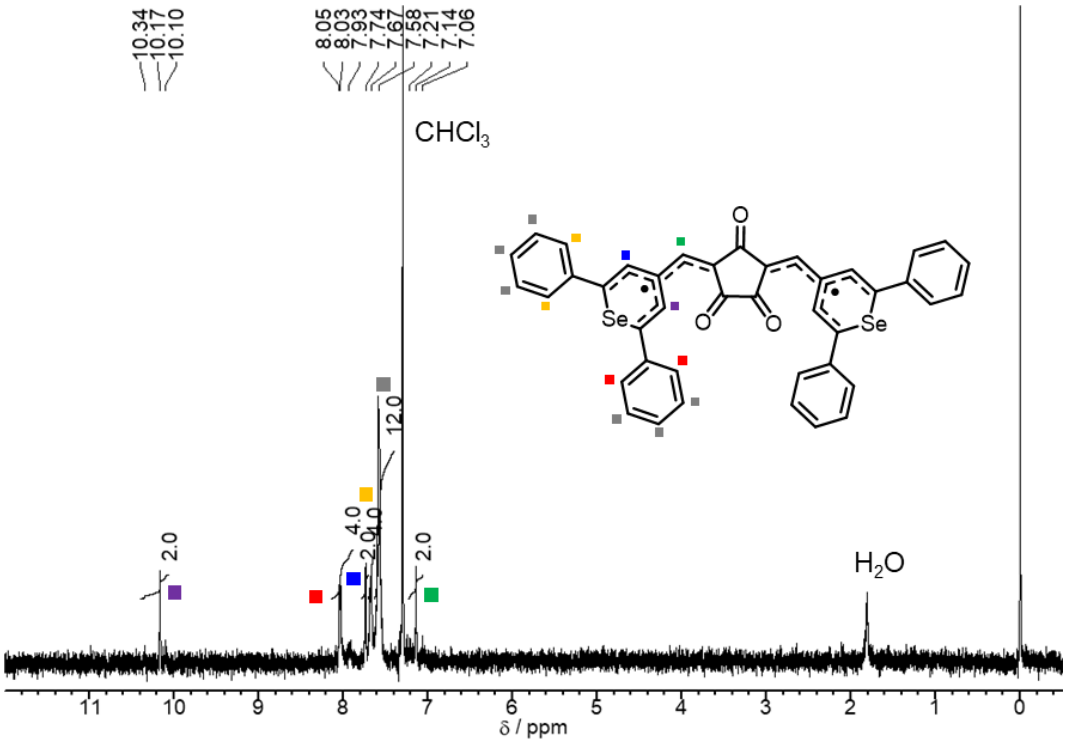

Fig. S19 ^{1}H NMR spectrum ($CDCl_3$, 213K) of **CR2c**.

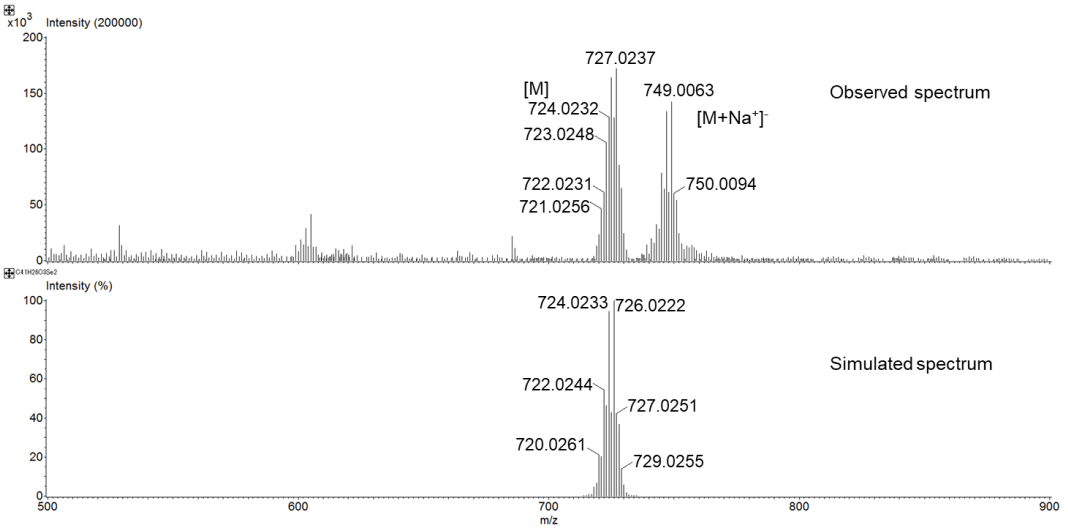

Fig. S20 ESI-MS spectrum of **CR2c** (top) and its corresponding simulated spectrum (bottom).

11. **Cartesian Coordinates of quantum chemical calculations**

Table S6. Optimized Cartesian coordinates of **CR2a** calculated at the CAM-B3LYP/6-31G(d,p) level with PCM solvation model ($CHCl_3$).

O	0.000004	-2.749917	-0.000037	C	-8.391942	-4.305866	-0.377394
O	1.401917	1.759650	-0.048615	C	-9.598151	-3.799554	0.097172
O	-1.401940	1.759640	0.048648	C	-9.670160	-2.479973	0.530053
C	5.439263	0.939241	0.011622	C	-8.543891	-1.669304	0.494090
C	4.133597	0.577024	0.020329	C	-5.961266	2.312742	-0.035700
C	3.757880	-0.800728	-0.004646	C	-5.146117	3.389444	0.332581
C	4.841279	-1.735639	-0.020051	C	-5.640964	4.684637	0.296751
C	6.129981	-1.321264	-0.006021	C	-6.952751	4.924464	-0.101292
C	2.443745	-1.293999	-0.010930	C	-7.769336	3.859000	-0.464176
C	1.204771	-0.670649	-0.006605	C	-7.280423	2.560295	-0.431100
C	0.000000	-1.521120	-0.000022	H	3.358961	1.332173	0.055333
C	0.765147	0.711432	-0.016737	H	4.629487	-2.796576	-0.058835
C	-0.765163	0.711426	0.016725	H	2.360839	-2.379452	-0.016100
C	-1.204778	-0.670657	0.006579	H	-2.360835	-2.379470	0.016109
C	-2.443747	-1.294018	0.010933	H	-4.629503	-2.796592	0.058855
C	-6.129984	-1.321267	0.006054	H	-3.358949	1.332150	-0.055369
C	-4.841285	-1.735652	0.020077	H	4.127415	3.215599	-0.660481
C	-3.757880	-0.800747	0.004657	H	4.999969	5.510160	-0.587869
C	-4.133586	0.577008	-0.020336	H	7.337057	5.938999	0.126530
C	-5.439248	0.939240	-0.011609	H	8.792543	4.038742	0.777755
C	5.961288	2.312737	0.035703	H	7.917221	1.734124	0.724275
C	5.146144	3.389431	-0.332606	H	6.335089	-3.898567	0.811707
C	5.640991	4.684625	-0.296797	H	8.331010	-5.331191	0.727063
C	6.952772	4.924460	0.101259	H	10.480168	-4.431088	-0.125005
C	7.769352	3.859001	0.464178	H	10.607419	-2.079319	-0.902066
C	7.280440	2.560296	0.431119	H	8.601319	-0.644598	-0.841820
C	7.326595	-2.174224	-0.024728	H	-6.335146	-3.898507	-0.811841
C	7.263149	-3.500500	0.416377	H	-8.331084	-5.331120	-0.727224
C	8.391894	-4.305913	0.377309	H	-10.480200	-4.431046	0.124983
C	9.598127	-3.799586	-0.097182	H	-10.607396	-2.079329	0.902206
C	9.670166	-2.479977	-0.529971	H	-8.601280	-0.644626	0.841985
C	8.543906	-1.669296	-0.493990	H	-4.127386	3.215621	0.660454
C	-7.326605	-2.174218	0.024752	H	-4.999940	5.510178	0.587801
C	-7.263188	-3.500463	-0.416449	H	-7.337035	5.939004	-0.126579

H	-8.792533	4.038733	-0.777742	O	-1.401940	1.759640	0.048648
H	-7.917207	1.734115	-0.724229	C	5.439263	0.939241	0.011622
O	-6.428679	0.004724	-0.000416	C	4.133597	0.577024	0.020329
O	6.428682	0.004721	0.000451	C	3.757880	-0.800728	-0.004646
O	0.000004	-2.749917	-0.000037	C	4.841279	-1.735639	-0.020051
O	1.401917	1.759650	-0.048615	C	6.129981	-1.321264	-0.006021

Table S7. Optimized Cartesian coordinates of **CR2b** calculated at the CAM-B3LYP/6-31G(d,p) level with PCM solvation model ($CHCl_3$).

O	-0.001191	-2.598823	-0.127750	C	7.129839	-2.555194	0.048847
O	1.401882	1.907092	0.050384	C	6.857214	-3.736699	0.748835
O	-1.397100	1.903392	0.150766	C	7.772824	-4.779448	0.754160
C	5.397256	1.179872	-0.006150	C	8.978653	-4.656794	0.071078
C	4.130394	0.691937	-0.067096	C	9.262660	-3.484084	-0.619440
C	3.771026	-0.689990	-0.047204	C	8.347913	-2.439229	-0.630193
C	4.797642	-1.687733	-0.032787	C	-7.128262	-2.558038	-0.005962
C	6.133868	-1.461073	0.031990	C	-6.873257	-3.731643	-0.725790
C	2.439905	-1.153741	-0.074052	C	-7.785536	-4.777231	-0.715629
C	1.208159	-0.522886	-0.053980	C	-8.972005	-4.665408	0.002103
C	-0.000323	-1.372693	-0.075937	C	-9.239338	-3.500456	0.712076
C	0.768652	0.858952	0.018546	C	-8.326881	-2.453540	0.708625
C	-0.765472	0.858219	0.056492	C	-5.689464	2.632808	-0.031563
C	-1.207521	-0.522251	-0.025866	C	-4.829067	3.511868	0.638058
C	-2.440092	-1.151359	-0.037539	C	-5.081050	4.876131	0.643486
C	-6.135553	-1.460582	-0.010974	C	-6.197752	5.386762	-0.010526
C	-4.797133	-1.684612	-0.011515	C	-7.060104	4.522543	-0.675284
C	-3.771200	-0.686531	-0.027374	C	-6.809771	3.156645	-0.687018
C	-4.129990	0.695752	-0.042441	H	3.318832	1.406025	-0.155067
C	-5.398832	1.181584	-0.034352	H	4.478721	-2.723057	-0.101395
C	5.687729	2.630778	-0.019488	H	2.335925	-2.237529	-0.100322
C	4.778068	3.527977	0.555278	H	-2.337355	-2.235202	-0.065636
C	5.030984	4.891773	0.542738	H	-4.473644	-2.720140	0.021250
C	6.197173	5.385128	-0.033972	H	-3.316336	1.412446	-0.073188
C	7.108165	4.503532	-0.603999	H	3.873736	3.154244	1.022196
C	6.857242	3.137675	-0.597960	H	4.315715	5.571550	0.993988

H	6.394532	6.452201	-0.038633	H	-4.404250	5.542152	1.168613
H	8.016715	4.878977	-1.063434	H	-6.394672	6.453877	-0.001887
H	7.567099	2.466469	-1.069958	H	-7.929264	4.911933	-1.195347
H	5.931617	-3.829273	1.306891	H	-7.479397	2.500199	-1.233277
H	7.547919	-5.686962	1.304983	S	-6.814416	0.151149	-0.015626
H	9.695575	-5.471420	0.079631	S	6.804841	0.149421	0.143887
H	10.198690	-3.381692	-1.158714	O	-0.001191	-2.598823	-0.127750
H	8.572872	-1.538842	-1.192411	O	1.401882	1.907092	0.050384
H	-5.964507	-3.816254	-1.311934	O	-1.397100	1.903392	0.150766
H	-7.573249	-5.678355	-1.281742	C	5.397256	1.179872	-0.006150
H	-9.686764	-5.481960	0.005203	C	4.130394	0.691937	-0.067096
H	-10.160165	-3.405777	1.278251	C	3.771026	-0.689990	-0.047204
H	-8.539685	-1.561313	1.288526	C	4.797642	-1.687733	-0.032787
H	-3.964794	3.122980	1.164707	C	6.133868	-1.461073	0.031990

Table S8. Optimized Cartesian coordinates of **CR2c** calculated at the CAM-B3LYP/6-31G(d,p) level with PCM solvation model ($CHCl_3$).

Se	6.886665	0.156333	0.185908	C	-4.779021	-1.703599	-0.014627
Se	-6.905445	0.170202	-0.035139	C	-3.761025	-0.690728	-0.060241
O	-0.002874	-2.591414	-0.174351	C	-4.109984	0.697094	-0.097839
O	1.396039	1.917153	0.037488	C	-5.359400	1.224665	-0.093505
O	-1.402824	1.909805	0.150992	C	5.602555	2.673015	0.054717
C	5.356534	1.216749	0.029786	C	4.688856	3.527349	0.684795
C	4.105800	0.696004	-0.051485	C	4.907000	4.897233	0.705874
C	3.755317	-0.690426	-0.072167	C	6.038398	5.437834	0.102970
C	4.770865	-1.704923	-0.090313	C	6.949871	4.598893	-0.528404
C	6.112033	-1.529555	-0.013383	C	6.734909	3.227633	-0.554515
C	2.427744	-1.150405	-0.110544	C	7.065044	-2.657909	-0.031932
C	1.194251	-0.513118	-0.080256	C	6.769238	-3.842298	0.652777
C	-0.004182	-1.359954	-0.112316	C	7.654563	-4.910739	0.623191
C	0.753303	0.871702	0.000050	C	8.848247	-4.812580	-0.084713
C	-0.760724	0.868251	0.041610	C	9.151736	-3.639238	-0.766600
C	-1.199734	-0.513761	-0.059451	C	8.268707	-2.568275	-0.740771
C	-2.436594	-1.151943	-0.070389	C	-7.070097	-2.655605	0.060635
C	-6.120566	-1.524472	0.007694	C	-6.821555	-3.817645	-0.678849

C	-7.697795	-4.892253	-0.616217	H	5.851726	-3.915669	1.226974
C	-8.835137	-4.824032	0.181991	H	7.415289	-5.820071	1.164857
C	-9.092915	-3.672414	0.917554	H	9.540630	-5.647995	-0.103536
C	-8.218382	-2.595643	0.858859	H	10.077280	-3.558013	-1.327105
C	-5.593903	2.683935	-0.113977	H	8.501420	-1.661288	-1.290305
C	-4.686815	3.545963	0.515639	H	-5.949378	-3.868450	-1.322017
C	-4.891530	4.918082	0.499016	H	-7.494225	-5.783924	-1.200264
C	-6.003710	5.455249	-0.141109	H	-9.519978	-5.664603	0.227803
C	-6.909548	4.609141	-0.770894	H	-9.974297	-3.613655	1.547797
C	-6.707766	3.235648	-0.758851	H	-8.415309	-1.708717	1.453527
H	3.279203	1.396432	-0.125346	H	-3.822126	3.138526	1.027220
H	4.423080	-2.728052	-0.199349	H	-4.179520	5.569886	0.994619
H	2.316509	-2.231814	-0.155216	H	-6.162569	6.528694	-0.150492
H	-2.325877	-2.234036	-0.093044	H	-7.774216	5.019272	-1.282458
H	-4.428313	-2.730354	0.035123	H	-7.409713	2.591014	-1.279230
H	-3.277562	1.392514	-0.138792	Se	6.886665	0.156333	0.185908
H	3.809319	3.114745	1.166396	Se	-6.905445	0.170202	-0.035139
H	4.190946	5.544580	1.201418	O	-0.002874	-2.591414	-0.174351
H	6.207600	6.509546	0.123194	O	1.396039	1.917153	0.037488
H	7.828619	5.013345	-1.011655	O	-1.402824	1.909805	0.150992
H	7.439724	2.584006	-1.072123	C	5.356534	1.216749	0.029786

Table S9. Optimized Cartesian coordinates of **CR2c** at the CAM-UB3LYP/6-31G(d,p) level with PCM solvation model ($CHCl_3$).

Se	6.902481	0.161416	0.207227	C	1.206791	-0.498968	-0.072491
Se	-6.925144	0.163471	0.008381	C	-0.003387	-1.346981	-0.094945
O	-0.005552	-2.573006	-0.150131	C	0.768390	0.883097	0.000009
O	1.400940	1.931738	0.025308	C	-0.766379	0.883386	0.047826
O	-1.394786	1.929662	0.150893	C	-1.210581	-0.495971	-0.039765
C	5.378640	1.224374	-0.042092	C	-2.441677	-1.127169	-0.058944
C	4.127151	0.702147	-0.106814	C	-6.129311	-1.531370	-0.037349
C	3.772512	-0.681387	-0.054578	C	-4.783579	-1.694544	-0.052821
C	4.778288	-1.702191	-0.016309	C	-3.778222	-0.673484	-0.039761
C	6.120755	-1.533969	0.064181	C	-4.130422	0.711204	-0.016320
C	2.436093	-1.134080	-0.083312	C	-5.383621	1.232616	0.006286

C	5.634693	2.677448	-0.111214	H	-4.423578	-2.719456	-0.054611
C	4.706189	3.582117	0.420041	H	-3.303289	1.413761	-0.029260
C	4.932904	4.948826	0.346494	H	3.807381	3.211708	0.900390
C	6.089482	5.438577	-0.252254	H	4.203918	5.634336	0.766182
C	7.017040	4.550129	-0.784313	H	6.266013	6.508048	-0.304734
C	6.792354	3.181592	-0.717051	H	7.916715	4.922758	-1.263223
C	7.069058	-2.665745	0.089072	H	7.510841	2.498288	-1.159376
C	6.759389	-3.833773	0.795846	H	5.834567	-3.889668	1.360261
C	7.637807	-4.908397	0.799789	H	7.385832	-5.804487	1.357641
C	8.840930	-4.833202	0.105109	H	9.528262	-5.672949	0.112546
C	9.159768	-3.675998	-0.596910	H	10.092904	-3.611801	-1.147078
C	8.282562	-2.599773	-0.605761	H	8.527861	-1.706546	-1.172024
C	-7.068502	-2.671624	-0.066021	H	-5.879598	-3.821246	-1.446210
C	-6.778071	-3.802677	-0.838642	H	-7.405046	-5.753961	-1.463161
C	-7.643578	-4.887558	-0.854771	H	-9.493382	-5.708197	-0.122713
C	-8.815939	-4.860614	-0.106340	H	-10.026654	-3.712522	1.251029
C	-9.117265	-3.739965	0.659625	H	-8.486234	-1.794819	1.302447
C	-8.252049	-2.654146	0.681330	H	-3.883052	3.110180	1.238291
C	-5.631288	2.688780	0.049752	H	-4.262436	5.537806	1.303076
C	-4.742943	3.531681	0.729788	H	-6.239446	6.526623	0.172753
C	-4.960710	4.901382	0.769263	H	-7.820648	5.051919	-1.044639
C	-6.069548	5.455398	0.137587	H	-7.429571	2.628599	-1.142938
C	-6.958198	4.628461	-0.540131	Se	6.902481	0.161416	0.207227
C	-6.741897	3.257699	-0.585676	Se	-6.925144	0.163471	0.008381
H	3.305742	1.400444	-0.228625	O	-0.005552	-2.573006	-0.150131
H	4.424308	-2.726978	-0.086037	O	1.400940	1.931738	0.025308
H	2.324487	-2.217318	-0.100490	O	-1.394786	1.929662	0.150893
H	-2.331972	-2.209815	-0.103189	C	5.378640	1.224374	-0.042092

Table S10. Optimized Cartesian coordinates of **CR2c** calculated at the CAM-UB3LYP/6-31G(d, p) level for triplet state with PCM solvation model ($CHCl_3$).

Se	-6.902482	0.161416	-0.207227	O	1.394786	1.929662	-0.150893
Se	6.925144	0.163471	-0.008381	C	-5.378640	1.224374	0.042092
O	0.005552	-2.573006	0.150131	C	-4.127151	0.702147	0.106814
O	-1.400940	1.931738	-0.025308	C	-3.772512	-0.681387	0.054578

C	-4.778289	-1.702191	0.016309	C	6.069549	5.455398	-0.137587
C	-6.120755	-1.533970	-0.064181	C	6.958198	4.628461	0.540131
C	-2.436093	-1.134080	0.083312	C	6.741897	3.257700	0.585676
C	-1.206791	-0.498968	0.072491	H	-3.305742	1.400445	0.228625
C	0.003387	-1.346981	0.094945	H	-4.424308	-2.726979	0.086037
C	-0.768390	0.883097	-0.000009	H	-2.324487	-2.217318	0.100490
C	0.766380	0.883386	-0.047826	H	2.331972	-2.209816	0.103189
C	1.210581	-0.495971	0.039765	H	4.423579	-2.719456	0.054611
C	2.441677	-1.127169	0.058944	H	3.303290	1.413761	0.029260
C	6.129311	-1.531370	0.037349	H	-3.807381	3.211708	-0.900390
C	4.783579	-1.694544	0.052821	H	-4.203919	5.634336	-0.766182
C	3.778222	-0.673484	0.039761	H	-6.266013	6.508048	0.304734
C	4.130422	0.711204	0.016320	H	-7.916716	4.922758	1.263223
C	5.383621	1.232616	-0.006286	H	-7.510842	2.498288	1.159376
C	-5.634694	2.677448	0.111214	H	-5.834567	-3.889668	-1.360261
C	-4.706190	3.582118	-0.420041	H	-7.385833	-5.804488	-1.357641
C	-4.932904	4.948826	-0.346494	H	-9.528263	-5.672949	-0.112546
C	-6.089482	5.438577	0.252254	H	-10.092905	-3.611802	1.147078
C	-7.017040	4.550129	0.784313	H	-8.527861	-1.706546	1.172024
C	-6.792354	3.181592	0.717051	H	5.879598	-3.821246	1.446210
C	-7.069059	-2.665745	-0.089072	H	7.405046	-5.753962	1.463161
C	-6.759390	-3.833773	-0.795846	H	9.493383	-5.708197	0.122713
C	-7.637808	-4.908397	-0.799789	H	10.026655	-3.712523	-1.251029
C	-8.840931	-4.833203	-0.105109	H	8.486234	-1.794819	-1.302447
C	-9.159768	-3.675999	0.596910	H	3.883052	3.110180	-1.238291
C	-8.282562	-2.599773	0.605761	H	4.262437	5.537807	-1.303076
C	7.068503	-2.671624	0.066021	H	6.239446	6.526624	-0.172753
C	6.778072	-3.802677	0.838642	H	7.820649	5.051920	1.044639
C	7.643578	-4.887559	0.854771	H	7.429572	2.628599	1.142938
C	8.815940	-4.860614	0.106340	Se	-6.902482	0.161416	-0.207227
C	9.117266	-3.739965	-0.659625	Se	6.925144	0.163471	-0.008381
C	8.252050	-2.654147	-0.681330	O	0.005552	-2.573006	0.150131
C	5.631288	2.688780	-0.049752	O	-1.400940	1.931738	-0.025308
C	4.742944	3.531682	-0.729788	O	1.394786	1.929662	-0.150893
C	4.960711	4.901382	-0.769263	C	-5.378640	1.224374	0.042092

References

1. Y. F. Qiu, F. Yang, Z. H. Qiu, M. J. Zhong, L. J. Wang, Y. Y. Ye, B. Song, Y. M. Liang, *J. Org. Chem.* 2013, **78**, 12018–12028.
2. L. Birzan, M. Cristea, C. Draghici, V. Tecuceanu, M. Maganu, A. C. Razus, *Rev. Chim.* 2020, **71**, 89–95.
3. SIR2004: M. C. Burla, R. Caliandro, M. Camalli, B. Carrozzini, G. L. Cascarano, L. De Caro, C. Giacovazzo, G. Polidori, R. Spagna R. *J. Appl. Cryst*. 2005, **38**, 381–388.
4. CrystalStructure 4.3: Crystal Structure Analysis Package, Rigaku Corporation (2000–2018), Tokyo 196-8666, Japan.
5. Bleaney, K. D. Bowers, *Proc. R. Soc. London Ser. A* **1952**, *214*, 451–465.
6. M. Sheik-Bahae, A. A. Said, T. H. Wei, D. J. Hagan, E. W. Van Stryland, *IEEE J. Quantum Electron.* 1990, **26**, 760–769.
7. K. Kamada, K. Matsunaga, A. Yoshino, K. Ohta, *J. Opt. Soc. Am. B* 2003, **20**, 529–537.
8. Gaussian 16, Revision C.01, M. J. Frisch, G. W. Trucks, H. B. Schlegel, G. E. Scuseria, M. A. Robb, J. R. Cheeseman, G. Scalmani, V. Barone, G. A. Petersson, H. Nakatsuji, X. Li, M. Caricato, A. V. Marenich, J. Bloino, B. G. Janesko, R. Gomperts, B. Mennucci, H. P. Hratchian, J. V. Ortiz, A. F. Izmaylov, J. L. Sonnenberg, D. Williams-Young, F. Ding, F. Lipparini, F. Egidi, J. Goings, B. Peng, A. Petrone, T. Henderson, D. Ranasinghe, V. G. Zakrzewski, J. Gao, N. Rega, G. Zheng, W. Liang, M. Hada, M. Ehara, K. Toyota, R. Fukuda, J. Hasegawa, M. Ishida, T. Nakajima, Y. Honda, O. Kitao, H. Nakai, T. Vreven, K. Throssell, J. A. Montgomery, Jr., J. E. Peralta, F. Ogliaro, M. J. Bearpark, J. J. Heyd, E. N. Brothers, K. N. Kudin, V. N. Staroverov, T. A. Keith, R. Kobayashi, J. Normand, K. Raghavachari, A. P. Rendell, J. C. Burant, S. S. Iyengar, J. Tomasi, M. Cossi, J. M. Millam, M. Klene, C. Adamo, R. Cammi, J. W. Ochterski, R. L. Martin, K. Morokuma, O. Farkas, J. B. Foresman, and D. J. Fox, Gaussian, Inc., Wallingford CT, 2019.
9. S. Hirata, M. Head-Gordon, *Chem. Phys. Lett.* 1999, **314**, 291–299.

10. K. Ohta, S. Yamada, K. Kamada, A. D. Slepkov, F. A. Hegmann, R. R. Tykwinski, L. D. Shirtcliff, M. M. Haley, P. Sałek, F. Gel'mukhanov, H. Ågren, *J. Phys. Chem. A* 2011, **115**, 105–117.
11. T. Maeda, T. Oka, D. Sakamaki, H. Fujiwara, N. Suzuki, S. Yagi, T. Konishi, K. Kamada, *Chem. Sci.* 2023, **14**, 1978–1985.
12. S. Webster, J. Fu, L. A. Padilha, O. V. Przhonska, D. J. Hagan, E. W. Van Stryland, M. V. Bondar, Y. L. Slominsky, A. D. Kachkovski, *Chem. Phys.* 2008, **348**, 143–151.
13. B. T. Makowski, B. Valle, K. D. Singer, C. Weder, *J. Mater. Chem.* 2012, **22**, 2848–2850.
14. T. Liu, M. V. Bondar, K. D. Belfield, D. Anderson, A. E. Masunov, D. J. Hagan, E. W. Van Stryland, *J. Phys. Chem. C* 2016, **120**, 11099–11110.
15. S.-J. Chung, S. Zheng, T. Odani, L. Beverina, J. Fu, L. A. Padilha, A. Biesso, J. M. Hales, X. Zhan, K. Schmidt, A. Ye, E. Zojer, S. Barlow, D. J. Hagan, E. W. Van Stryland, Y. Yi, Z. Shuai, G. A. Pagani, J.-L. Brédas, J. W. Perry, S. R. Marder, *J. Am. Chem. Soc.* 2006, **128**, 14444–14445.
16. Q. Shi, W.-Q. Chen, J. Xiang, X.-M. Duan, X. Zhan, *Macromolecules* 2011, **44**, 3759–3765.
17. S. Webster, S. A. Odom, L. A. Padilha, O. V. Przhonska, D. Peceli, H. Hu, G. Nootz, A. D. Kachkovski, J. Matichak, S. Barlow, H. L. Anderson, S. R. Marder, D. J. Hagan, E. W. Van Stryland, *J. Phys. Chem. B* 2009, **113**, 14854–14867.
18. H.-J. Chang, M. V. Bondar, T. Liu, X. Liu, S. Singh, K. D. Belfield, A. Sheely, A. E. Masunov, D. J. Hagan, E. W. Van Stryland, *ACS Omega*, 2019, **4**, 14669–14679.